Indentation parameters for Brinell hardness measurement of low carbon steels

A.V. Udalov[1*], *A.A.* Udalov[2], and *E.G.* Norin[1]

[1] Vyatka State University, 36 Moskovskaya St., Kirov, 610000, Russian Federation
[2] Ural Federal University named after the First President of Russia B.N. Yeltsin, 19 Mira St., Ekaterinburg, 620002, Russian Federation

Abstract. Brinell hardness of steel 20 was measured with a ball of constant diameter according to the standard technique *D=10 mm* at different test load values from the range *F=62.5…3000 kgf*. The diameter *d* of the reconstructed indentation was measured. According to the developed method the deformation resistance of the sample material in the plastic zone bounded by a hemisphere was determined. The highest values of deformation resistance were recorded at indentation up to the ratio of *d/D=0.245*. Based on the results obtained, it is recommended to measure the Brinell hardness of steel 20 at the degree of loading $F/D^2=5$. During the ball indentation process, the sample material undergoes significant deformation, which must be taken into account when measuring hardness.

1 Introduction

Standard methods of hardness determination under static application of a measuring load (Brinell, Rockwell, Super-Rockwell, Vickers methods) are very widely used to control the mechanical characteristics of the material in the manufacturing technologies of various parts [1-3], as well as for diagnostics of the performance of structural elements [4-11]. At the same time, the accuracy of hardness measurement is largely affected by the indentation size effect (ISE), which manifests itself in the change of the fixed hardness depending on the indentation conditions (the value of the test load and the indenter indentation depth, as well as its shape and dimensions). The scientific community has made considerable efforts to study ISE [12-16] and to establish the basic regularities between fixation hardness and indentation conditions [17-23]. At the same time in practice quite often there are situations when in order to control the properties of a material having a given mechanical characteristics it is possible to use two or more methods of hardness measurement on different scales. In some cases it is quite difficult to make a correct choice of the most rational method. Of course, there are general recommendations on the choice of a particular method (approximate range of hardness numbers of the method, dimensions and shape of the sample, as well as indentation zones), but all of them are mainly qualitative in nature. But if we talk about hardness as a mechanical characteristic, it is mostly the ability to resist elastic and plastic deformations during indentation of the indenter. This ability is assessed

* Corresponding author: a.v.udalov1960@gmail.com

by standard methods by the size of the residual indentation or the depth of indentation of the indenter, which are in fact only external signs and a consequence of changes in the material in the deformation zone during the hardness measurement process. Using only geometric parameters of the reconstructed indentation it is practically impossible to compare in any way the hardness numbers on different scales and to make a conclusion about their preference. Therefore, tables of hardness scale ratios are made only on the basis of direct measurements [24].

The main quantitative criterion to assess the ability to resist plastic deformation is the resistance to deformation of the material. But in the scientific and technical literature devoted to the study of hardness measurement methods, there are no simple engineering methods that allow, depending on various factors, to determine accurately enough the deformation resistance of the material in the center of deformation under the indenter. It should be noted that we are not talking about the deformation resistance of the base metal of the sample from the non-deformable zone, the hardness of which is estimated by the specific pressure on the contact surface of the indenter. We are talking about resistance to deformation in the deformation center created by indentation of the indenter. Therefore, in this case the use of generally accepted empirical relationships between hardness and deformation resistance is not possible, because the experimental determination of the hardness of the material exactly in the deformation center is associated with sufficiently large technical difficulties. The use of the finite element method (FEM) to study the deformation center still requires considerable time, money and effort, so not all researchers can apply the FEM in practice. Thus, the resistance to deformation just in the deformation center under the indenter can become a general quantitative criterion for evaluating the ability of a material to resist plastic deformation, by which one can judge the preference of any method of hardness measurement.

The purpose of the paper is to develop an engineering method for determining the deformation resistance of a material in the deformation zone arising during indentation of an indenter depending on various parameters of the static indentation process.

The study was carried out on the example of measuring Brinell hardness of steel 20 under different loads with a ball of constant diameter. In the work devoted to the study of the hardness measurement process [16] it was established that the main criteria for the manifestation of the dimensional effect are the specific work of plastic deformation and the ratio of the specific work to the degree of deformation of the material in the indentation process. At the same time, the ratio of specific work to the degree of deformation is proportionally reflected in the change of deformation resistance of the material in the deformation center during indentation. In the presented study for steel 20 the main parameters of the deformation center (specific work of plastic deformation and deformation resistance of the material) arising in the process of indentation are determined according to the results of hardness measurement. On the basis of the obtained results, practical recommendations are given on the assignment of a rational value of the degree of loading, which should be applied to measure the Brinell hardness of steel 20.

2. Methods and Results

The scheme of Brinell hardness measurement with the parameters of the emerging deformation center is shown in Fig. 1. The geometry of the deformation zone is developed using the sliding cone theory [14-16], in accordance with which all the work of plastic deformation during ball indentation is spent on plastic molding of the material inside the sliding cone *ACB*. The sliding cone is bounded on one side by the contact surface of the ball, and on the other side by the lines of main shear stresses *AC* and *CB* forming the cone.

Hardness measurement was performed according to the standard method on samples made of steel 20 (analog: steel 1020 - USA) subjected to annealing. Yield strength of steel 20 after annealing $\sigma_{S0} = 280\ MPa$.

The initial data for calculation of the ball indentation process parameters (specific work and resistance to material deformation) were: *D* - ball diameter, *mm*; *F* - test load, *kgf*; *d* - diameter of the reconstructed ball indentation, *mm*.

Calculations of the deformation center parameters were performed by the diameter of the restored indentation d, which was measured after indentation with a Brinell magnifying glass with an accuracy of 0.05 mm.

Hardness of initial samples from steel 20 on the standard Brinell scale at the degree of loading $F/D^2 = 10$ equals approximately *115 HB10/1000*.

Brinell hardness measurement was performed with a ball of constant diameter *D=10 mm* at different values of test load in the range from 62.5 to 3000 *kgf* (Table 1).

The calculated values were the following parameters.

Degree of loading, *kgf/mm²*

$$K_F = F/D^2 \ . \tag{1}$$

Coefficient of imprint diameter

$$K_d = d/D \ . \tag{2}$$

Angle of contact of the ball with the sample (Fig.1), *degree*

$$\alpha = 2 \cdot arcSin\frac{d}{D} . \tag{3}$$

Print depth, *mm*

$$h = \frac{D}{2} \cdot \left(1 - Co\frac{\alpha}{2}\right) . \tag{4}$$

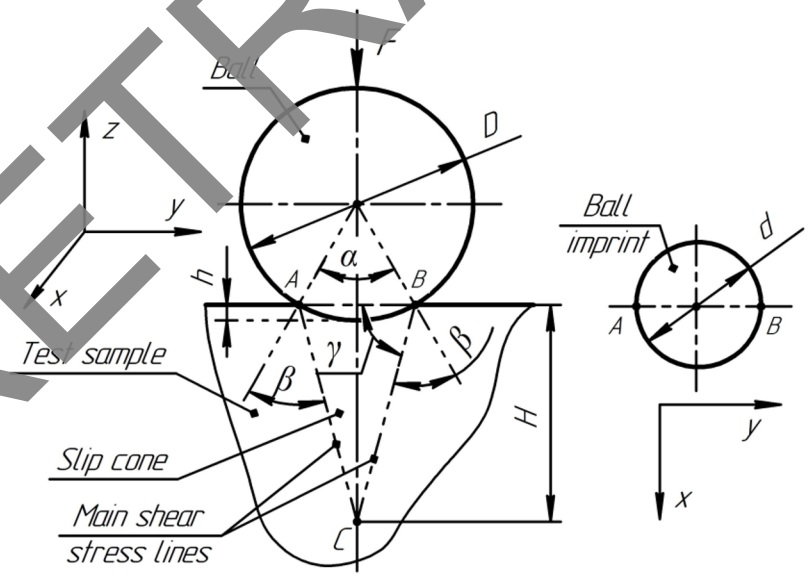

Fig.1. Brinell hardness measurement scheme with parameters of the deformation center in the form of a sliding cone

Angle of inclination of the main shear stress lines to the original surface of the sample, *degree*

$$\gamma = 180^o - \beta - \left(90^o - \alpha/2\right) = 45^0 + \frac{\alpha}{2} \ . \quad (5)$$

Here: β = 45° is the angle of inclination of the main shear stress lines to the normal of the indenter surface.

It is assumed that the pressure forces from the ball during indentation into the sample material are directed along the radius (normal to the indenter surface). In further calculations, the angle β is assumed to be constant regardless of the indenter shape, i.e., β = 45°.

Height of sliding cone *ACB*, *mm*

$$H = \frac{d}{2} \cdot tg\gamma \ . \quad (6)$$

Average value of the degree of deformation of the material inside the sliding cone *ACB* (Fig.1)

$$\varepsilon = \ln \frac{H}{H - h} \ . \quad (7)$$

In formula (7), the height of the sliding cone H for this model of the deformation center is actually the depth of plastic deformation propagation during ball indentation and is taken as the initial size of the deformed element. Accordingly, the depth of ball indentation h is taken as its absolute deformation.

The area of the contact surface of the ball and the specimen was assumed to be equal to the area of the ball segment with height h, *mm²*

$$S = \pi D h \ . \quad (8)$$

Specific pressure on the contact surface of the ball and sample, *MPa*

$$p = \frac{9,81 \cdot F}{S} \ . \quad (9)$$

Brinell hardness, *kgf/mm²*

$$HB = p/9,81 \ . \quad (10)$$

Volume of material displaced at ball indentation equal to volume of ball segment of height h, *mm³*

$$V_B = \frac{\pi h}{6}\left(0,75d^2 + h^2\right) , \quad (11)$$

The work of plastic deformation when the ball is pushed into the sample material is equal to the product of specific pressure by the volume of displaced material, *J*

$$A = p \cdot V_B \cdot 10^{-3} \ . \quad (12)$$

Calculated value of the slip cone volume *ACB* (deformation center) *(Fig.1)*, *mm³*

$$V = \frac{1}{3} \cdot \frac{\pi d^2}{4} \cdot H - V_B \ . \quad (13)$$

In accordance with the adopted model of the deformation center, work A is spent on plastic deformation of the material only within the *ACB* sliding cone.

Specific work of plastic deformation at ball indentation (work per unit volume of deformable material located inside the *ACB* sliding cone), *J/mm³*.

$$A_V = A/V \ . \quad (14)$$

Integral criterion of change of fixed hardness is the ratio of specific work A_V to the degree of deformation ε [16], which from the physical point of view is equal to the average value of deformation resistance of the material located under the indenter (in this case in the sliding cone *ACB*).

The strain resistance of the material in the deformation center is equal to the amount of specific work required to produce a unit of maximum principal strain ε inside the slip cone *ACB*, *MPa:*

$$\sigma_S = \frac{A_V}{\varepsilon} \cdot 10^3 . \tag{15}$$

The calculated values of the parameters of the deformation center in the form of slip cone *ACB* are given in Table 1. The presented results show a significant excess of the calculated values of the deformation resistance of the material σ_S over the specific pressure *p*. From a physical point of view, this ratio ($p < \sigma_S$) is impossible. For example, in the practice of metal forming processes, the condition of metal flow is the approximate ratio of $p \approx (2,6...3)\sigma_S$ [25]. Obviously, for the proposed model of the deformation zone based on the construction of sliding cones, the numerical values of the volume *V* are much smaller than the volume of the actual deformation zone.

The actual shape of the deformation center under the indenter is more of a hemisphere [26-30] with radius *R* (Fig. 2). The volume of the hemisphere corresponding to the actual shape of the deformation center under the ball indenter was determined by the formula, *mm*^{3}

$$V^R = V \cdot \frac{\sigma_S}{p} . \tag{16}$$

Actual value of specific work of plastic deformation in the hemisphere volume, *J/mm*^{3}.

$$A_V^R = A / V^R . \tag{17}$$

Radius of the hemisphere corresponding to the actual volume of the deformation center V^R

$$R = \sqrt[3]{\frac{3}{4} \cdot \frac{2 \cdot V^R}{\pi}} . \tag{18}$$

The hemisphere with radius *R* (Fig.2) is a conditional boundary of plastic deformation propagation during indentation of the indenter. The average value of the actual degree of deformation of the material in the deformation center bounded by the hemisphere was determined by the formula

$$\varepsilon^R = \ln \frac{R}{R-h} . \tag{19}$$

In formula (19), the radius of the hemisphere *R* actually determines the depth of plastic deformation propagation during ball indentation and is taken as the initial size of the deformed element. At the same time, the depth of ball indentation h is actually the absolute deformation of this element.

Average actual value of the resistance to deformation of the material in the volume of the hemisphere

$$\sigma_S^R = \frac{A_V^R}{\varepsilon^R} \cdot 10^3 . \tag{20}$$

Numerical values of parameters calculated by formulas (1)-(20) are given in Table 1. For clarity, figure 3 shows graphical dependences of specific pressure p and deformation resistance σ_S^R of the ball indentation depth expressed in the ratio d/D.

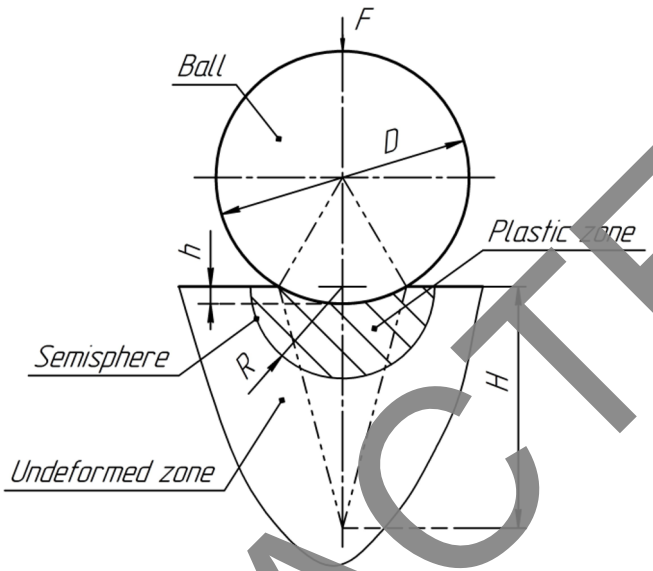

Fig. 2. Actual deformation center in the form of a hemisphere with radius R

Table 1. Numerical values of indentation parameters by Brinell (sample material - steel 20, heat treatment annealing)

Hardness scale	*D, mm*	*F, kgf*	*F/D²*	*d, mm*	*d/D*	$\frac{\varepsilon^*}{\varepsilon^R}$	*p, MPa*	*HB, kgf/mm²*	$\frac{A_V^*}{A_V^R}$	$\frac{\sigma_S^*}{\sigma_S^R}$
HB10/62.5	10	*62.5*	*0.625*	*1.3*	*0.13*	$\frac{0.051}{0.068}$	*460*	*47*	$\frac{0.038}{0.024}$	$\frac{728}{344}$
HB10/187.5		*187.5*	*1.875*	*1.70*	*0.170*	$\frac{0.062}{0.088}$	*804*	*82*	$\frac{0.080}{0.05}$	$\frac{1290}{567}$
HB10/250		*250*	*2.5*	*1.85*	*0.185*	$\frac{0.066}{0.096}$	*905*	*92*	$\frac{0.096}{0.06}$	$\frac{1456}{622}$
HB10/500		*500*	*5*	*2.45*	*0.245*	$\frac{0.077}{0.124}$	*1024*	*104*	$\frac{0.129}{0.079}$	$\frac{1674}{638}$
HB10/750		*750*	*7.5*	*2.9*	*0.29*	$\frac{0.082}{0.144}$	*1090*	*111*	$\frac{0.148}{0.090}$	$\frac{1796}{626}$
HB10/1000		*1000*	*10*	*3.25*	*0.325*	$\frac{0.085}{0.158}$	*1150*	*117*	$\frac{0.162}{0.098}$	$\frac{1905}{618}$
HB10/1250		*1250*	*12.5*	*3.60*	*0.36*	$\frac{0.086}{0.172}$	*1164*	*119*	$\frac{0.168}{0.100}$	$\frac{1935}{584}$
HB10/1500		*1500*	*15.0*	*3.90*	*0.390*	$\frac{0.086}{0.183}$	*1183*	*121*	$\frac{0.169}{0.101}$	$\frac{1970}{556}$
HB10/2000		*2000*	*20*	*4.40*	*0.44*	$\frac{0.083}{0.198}$	*1224*	*125*	$\frac{0.169}{0.101}$	$\frac{2042}{511}$
HB10/2500		*2500*	*25*	*4.80*	*0.48*	$\frac{0.078}{0.208}$	*1272*	*130*	$\frac{0.165}{0.099}$	$\frac{2119}{475}$

HB10/3000		*3000*	*30*	*5.20*	*0.52*	$\frac{0.071}{0.215}$	*1285*	*131*	$\frac{0.151}{0.091}$	$\frac{2133}{423}$

Note: * – in the numerator are the parameters of the deformation center in the form of a slip cone (Fig.1), and in the denominator for the actual deformation center in the form of a hemisphere (Fig. 2); A_V and A_V^R, *J/mm³*; σ_S and σ_S^R, *MPa*

The parameter values presented in Table 1 show a monotonic increase in the degree of deformation of the material ε^R, specific pressure *p* and fixed hardness *HB* with increasing test load *F*. In this case, the average value of the deformation resistance of the material σ_S^R varies non-monotonically taking an extreme value at the ratio $\frac{d}{D} \approx 0.245$ (Fig.3).

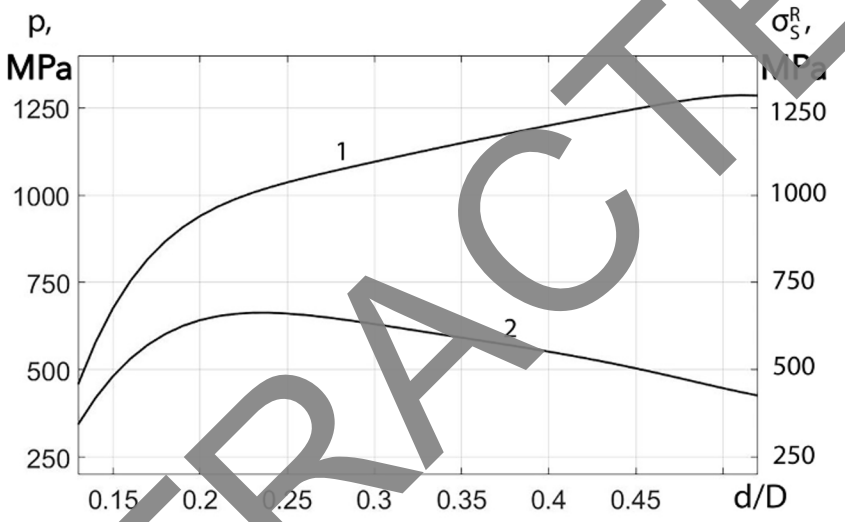

Fig. 3. Variation of specific pressure *p* and deformation resistance σ_S^R at different depths of ball indentation: 1 - graph of dependence $p - d/D$; 2 – graph of dependence $\sigma_S^R - d/D$

3 Discussion

The monotonic growth of the specific pressure *p* and, consequently, of the recorded hardness *HB* with increasing indentation depth (Fig.3) is explained by the more intensive growth of the test load *F*, due to increasing friction forces, compared to the increase of the contact surface *S*. This effect is solely due to the ball geometry.

In this case, for the hardness measurement process, a non-monotonic dependence between the deformation resistance is fixed σ_S^R depth of indentation *h* (Fig. 3), which is explained by the peculiarities of the indentation process.The main feature is the formation of a swell around the well due to displacement of the sample material from the deformation center. At the same time, the intensity of the swell formation changes as the indenter is pushed in. At the initial stage of indentation limited by the ratio of *d/D=0.245* deformation resistance σ_S^R is increased to the maximum value *638 MPa* (Table 1). At this stage, the sample material is under all-round non-uniform compression within a deformation center

bounded on the one hand by the material of the undeformed zone (Fig. 2), and on the other hand by the indenter and the outer layers of the sample. The resistance to deformation at the initial stage increases until plastic deformation begins to develop in the outer layers of the sample, followed by the formation of a swell. But until then, surface layers create a kind of surface tension forces capable of holding the material inside the plastic zone and preventing the formation of a swell. At this time, the surface layers of the sample experience mainly elastic deformations.

Indentation of the indenter to a depth with a ratio of $d/D>0.245$ causes the development of plastic deformation in the surface layers of the sample with the intensive formation of a swell around the well. From this point, the deformation resistance starts to decrease (Fig. 3), and the work of plastic deformation is additionally spent on the molding of the swell. As a result of the swell formation, the volume of the plastic zone and the diameter of the indentation d start to increase further. At the same time, the increasing swell does not allow the deformation resistance of the material in the plastic zone to grow. Moreover, the resistance to deformation of the material begins to decrease, i.e., the processes of de-hardening of the material in the plastic zone begin to take place. The monotonic increase of specific pressure p is explained by more intensive growth of friction forces on the contact surface of the indenter. In addition, the intensive movement of the material in the direction of the formed buildup leads to additional energy consumption associated with its mixing inside the plastic zone. Such processes, which are mainly related to the formation of the buildup, certainly cannot positively influence the accuracy of hardness measurement. From the point of view of obtaining stable results when measuring hardness, the sample material should receive the greatest possible degree of development during plastic deformation in order to reduce the anisotropy of the material. At this point, the sample material should have the highest value of strain resistance. According to the results of hardness measurement (Table 1) the highest values of deformation resistance are as follows: $\sigma_S^R = 638\ MPa$ correspond to the indentation depth at the ratio of diameters $d/D=0.245$.

Further indentation of the indenter will not bring additional effects on reducing the influence of anisotropy of the sample material on the measurement results, since the deformation resistance of the material only decreases, and the increasing swelling brings only additional errors related to the measurement of the indentation diameter and hardness.

Additionally, the obtained numerical values σ_S^R were used to determine the degree of deformation that the sample material receives during tensile tests providing the same level of stress. For this purpose, we used the known empirical dependence of the steel 20 hardening curve based on the results of standard tensile tests on samples with different degrees of pre-hardening (Russian Federation patent No. 2 703 808)

$$\sigma_S = 280 + 418{,}3 \cdot \left(\sqrt{3} \cdot \varepsilon\right)^{0{,}39}, \tag{21}$$

where ε – tensile strain of the cylindrical sample;

σ_S – yield strength of the sample material corresponding to the degree of deformation ε.

According to equation (21) the hardening curve is constructed (Fig. 4).

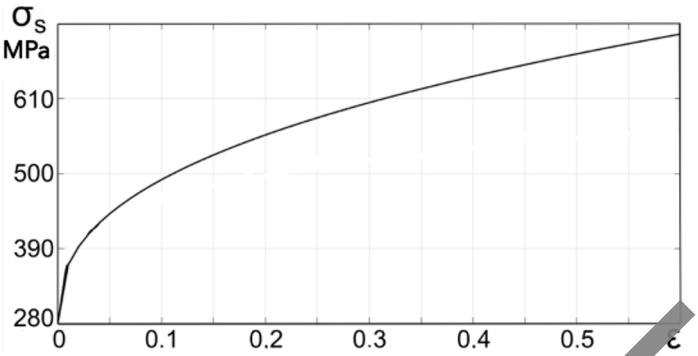

Fig. 4. Strengthening curve of steel 20 obtained by tensile testing of cylindrical samples.

The highest value of material deformation resistance during indentation is equal to $\sigma_S^R = 638\,MPa$ at the deformation degree $\varepsilon^R = 0.124$ (Table 1). According to the hardening curve (Fig. 4) stresses *638 MPa* correspond to a relative pre-hardening strain of approx. $\varepsilon \approx 0.4$. Thus, indentation causes significant plastic deformation that must be taken into account when measuring hardness. An example of a solution to this problem is a method of determining hardness without taking into account the hardening of the material caused by indentation of the indenter [31].

4 Conclusions

By measuring the Brinell hardness of steel 20 with a ball of diameter *D=10 mm* at loads from 62.5 kgf to 3000 kgf, the criteria and conditions ensuring the most reliable and stable measurement results are established.

The main criterion for selecting indentation conditions is the maximum value of material deformation resistance σ_S in the plastic zone, which contribute to the greatest extent to reducing the influence of material anisotropy and increasing the reliability of the hardness measurement result.

The highest values of resistance to deformation of the material in the plastic zone when measuring the hardness of steel 20 occur at a depth of indentation of the indenter providing the ratio of diameters *d/D=0.245*, which allows us to recommend for this steel the degree of loading which allows us to recommend for this steel the degree of loading $F/D^2=5$. During the ball indentation process, the sample material undergoes significant deformation, which must be taken into account when measuring hardness.

References

1. A. Rudnytskyj, M. Varga, S. Krenn, G. Vorlaufer, J. Leimhofer, M. Jech, C. Gachot, Internat. J. of Mechan. Sciences, **232**, 107571 (2022), https://doi.org/10.1016/j.ijmecsci.2022.107571.
2. D. G. Mevec, V. Jászfi, P. Prevedel, J. Todt, E. Maawad, J. Keckes, P. Raninger, Materials Today Communications, **33**, 104267 (2022), https://doi.org/10.1016/j.mtcomm.2022.104267.
3. S. Kucharski, S. Mackiewicz, T. Katz, G. Starzyński, Z. Ranachowski, S. Woźniacka, Internat. J. of Fatigue, **167 (B),** 107346 (2023), https://doi.org/10.1016/j.ijfatigue.2022.107346

4. G. Bolzon, Procedia Structural Integrity, **41**, 9–13 (2022), https://doi.org/10.1016/j.prostr.2022.05.003.
5. G. Bolzon, B. Rivolta, Engineer. Failure Analys, **90**, 434-439 (2018), https://doi.org/10.1016/j.engfailanal.2018.04.008
6. H. Xin, J. A.F.O. Correia, M. Veljkovic, F. Berto, L. Manuel, Internat. J.l of Fatigue, **147**, 106175 (2021), https://doi.org/10.1016/j.ijfatigue.2021.106175.
7. Š. Miroslav, C. Vladimír, M. Kepka, Procedia Structural Integrity, **7**, 262-267 (2017), https://doi.org/10.1016/j.prostr.2017.11.087.
8. I.E. Zvonarev, S.L. Ivanov, D.I. Shishlyannikov, Procedia Engineer., **150**, 618-625 (2016), https://doi.org/10.1016/j.proeng.2016.07.054.
9. M. P. Garcia, A. Gervasyev, C. Lu, F. J. Barbaro, Internat. J. of Pressure Vessels and Piping, **200**, 104837 (2022), https://doi.org/10.1016/j.ijpvp.2022.104837.
10. Z. Liu, L. Yang, G. Zhang, L. Zhao, Q. Shao, D. Huang, C. Zhu, Y. Wang, X. Shen, Z. Yang, H. Wang, Engineer. Failure Analys., **158**, 107994 (2024), https://doi.org/10.1016/j.engfailanal.2024.107994.
11. R. Bonetti, A. Morris, P.H. Shipway, W. Sun, Internat. J. of Pressure Vessels and Piping, **199**, 104735 (2022), https://doi.org/10.1016/j.ijpvp.2022.104735.
12. S. Kucharski, M. Maj, M. Ryś, H. Petryk, Internat. J. of Mechanical Sciences, **272**, 109138 (2024), https://doi.org/10.1016/j.ijmecsci.2024.109138.
13. M.A. Mattucci, I. Cherubin, P. Changizian, T. Skippon, M.R. Daymond, Acta Materialia, **207**, 116702 (2021), https://doi.org/10.1016/j.actamat.2021.116702.
14. A.A. Udalov, S.V. Parshin, A.V. Udalov, Materials Today: Proceedings, **19**, 2034 (2019), https://doi.org/10.1016/j.matpr.2019.07.068
15. A.A. Udalov, A.V. Udalov, S.V. Parshin, Solid State Phenomena, **299**, 1172 (2020), https://doi.org/10.4028/www.scientific.net/SSP.299.1172
16. A.V. Udalov, A.A. Udalov, E3S Web of Conf, **431**, 06025 (2023), https://doi.org/10.1051/e3sconf/202343106025
17. C. Barajas, J. de Vicente, J. Caja, P. Maresca, E. Gómez, Procedia Manufactur., **13**, 550-557 (2017), https://doi.org/10.1016/j.promfg.2017.09.089.
18. G. Leyi, Z. Wei, Z. Jing, H. Songling, Measurement, **44 (10),** 2129-2137 (2011), https://doi.org/10.1016/j.measurement.2011.07.024.
19. K. S. Kravchuk, A. A. Kostsova, D. Y. Kondratskiy, Materials Today: Proceedings**, 5** (12), 2, 26128-26132 (2018), https://doi.org/10.1016/j.matpr.2018.08.042.
20. P. Organek, B. Gosowski, M. Redecki, Structures, **59**, 105701 (2024), https://doi.org/10.1016/j.istruc.2023.105701.
21. É. Carvalho de Santana, W. Z. Misiolek, A. L.M. Costa, Internat. J. of Solids and Structures, **252**, 111817 (2022), https://doi.org/10.1016/j.ijsolstr.2022.111817.
22. F. Khodabakhshi, A. P. Gerlich, Materials Science and Engineer.: A, **789**, 139682 (2020), https://doi.org/10.1016/j.msea.2020.139682.
23. E. Broitman, Tribology Letters, **65 (1),** 23 (2017),
24. T. Yamamoto, M. Yamamoto, K. Miyahara, Measurement: Sensors, **18**, 100120 (2021), https://doi.org/10.1016/j.measen.2021.100120.
25. D. Tabor, The hardness of metals. – Oxford university press, 2000.
26. S. Sivaram, J.A.S.C. Jayasinghe, C.S. Bandara, Engineer: Journal of the Institution of Engineers, Sri Lanka, **54 (1),** 47–55 (2021), DOI: http://doi.org/10.4038/engineer.v54i1.7434

27. T. Zhang, J. Li, B. Yang, X. Pei, W. Jiang, Internat. J. of Pressure Vessels and Piping, **202**, 104886 (2023), https://doi.org/10.1016/j.ijpvp.2023.104886.
28. K. Liu, S. Gao, Z. Wang, X. Xiao, C. Jiang, J. of Materials Research and Technology, **27**, 2847-2855 (2023), https://doi.org/10.1016/j.jmrt.2023.10.101.
29. X. Li, W. Zhang, M. Han, F. Xie, D. Li, J. Zhang, B. Long, J. of Materials Research and Technology, **23**, 143-153 (2023), https://doi.org/10.1016/j.jmrt.2023.01.001.
30. A. G. Custodio, K. J. Lindquist, M. Tolentino, C. Aranas, G. C. Saha, J. of Alloys and Metallurg. Systems, **4**, 100043 (2023), https://doi.org/10.1016/j.jalmes.2023.100043.
31. A.V. Udalov, A.A. Udalov, Chernye Metally, **1**, 52–56 (2022), https://doi.org/10.17580/chm.2022.01.08.